AIP | Applied Physics Letters

Simulation of multilevel cell spin transfer switching in a full-Heusler alloy spin-valve nanopillar

H. B. Huang, X. Q. Ma, Z. H. Liu, C. P. Zhao, S. Q. Shi et al.

Citation: Appl. Phys. Lett. **102**, 042405 (2013); doi: 10.1063/1.4789867
View online: http://dx.doi.org/10.1063/1.4789867
View Table of Contents: http://apl.aip.org/resource/1/APPLAB/v102/i4
Published by the American Institute of Physics.

Simulation of multilevel cell spin transfer switching in a full-Heusler alloy spin-valve nanopillar

H. B. Huang,[1,2] X. Q. Ma,[1,a)] Z. H. Liu,[1] C. P. Zhao,[1] S. Q. Shi,[3] and L. Q. Chen[2]
[1]*Department of Physics, University of Science and Technology Beijing, Beijing 100083, China*
[2]*Department of Materials Science and Engineering, The Pennsylvania State University, University Park, Pennsylvania 16802, USA*
[3]*Department of Mechanical Engineering, The Hong Kong Polytechnic University, Hung Hom, Kowloon, Hong Kong*

(Received 27 September 2012; accepted 16 January 2013; published online 29 January 2013)

A multilevel cell spin transfer switching process in a full-Heusler $Co_2FeAl_{0.5}Si_{0.5}$ alloy spin-valve nanopillar was investigated using micromagnetic simulations. An intermediate state of two-step spin transfer magnetization switching was reported due to the four-fold magnetocrystalline anisotropy; however, we discovered the intermediate state has two possible directions of $-90°$ and $+90°$, which could not be detected in the experiments due to the same resistance of the $-90°$ state and the $+90°$ state. The domain structures were analyzed to determine the mechanism of domain wall motion and magnetization switching under a large current. Based on two intermediate states, we reported a multilevel bit spin transfer multi-step magnetization switching by changing the magnetic anisotropy in a full-Heusler alloy nanopillar. © *2013 American Institute of Physics*. [http://dx.doi.org/10.1063/1.4789867]

Spin transfer torque (STT), arising from the transfer of angular momentums from the electrons of the spin-polarized current to the ferromagnet, was initially proposed by Berger[1] and Slonczewski[2] in 1996. It could be utilized in magnetic devices.[3–6] One of the most attractive applications is high density magnetic random access memory (MRAM),[7,8] which has the advantage of large storage density, high addressing speed, low energy consumption, and avoidance of cross writing. However, the high critical switching current of STT-MRAM has to be reduced in order to achieve the compatibility with highly scaled complementary metal-oxide-semiconductor technology while maintaining the thermal stability. Recently, smaller critical current density was reported[9–11] in spin-valve nanopillars with half-metallic Heusler alloys because of its lower magnetization saturation M_s, smaller Gilbert damping constant α, and higher spin polarization factor η.[12–14] Another possible approach to increase the storage density is to store multiple bits per cell.[15–17] The combination of small critical current and multiple bits per cell in one device is the most desired path towards high density STT-MRAM.

Sukegawa *et al.*[14] demonstrated efficient spin transfer switching in $Co_2FeAl_{0.5}Si_{0.5}$ (CFAS)-based spin valve and showed that the resistance-current curves exhibited a two-step switching process, originating from the interplay between the magnetocrystalline anisotropy of CFAS layers and STT. Our simulations of CFAS layers[18] also showed a two-step switching domain evolution, and we explained the unsymmetrical resistance-current curves using the unsymmetrical STT. There exists an intermediate (I) state with the direction of the magnetization perpendicular to their original antiparallel (AP) and final parallel (P) spin configurations. However, we found the I state has two possible states, $-90°$ state and $90°$ state, which could not be detected due to the same resistance because of only two CFAS layers in the experiment.[14] In this paper, we will report a way of applying the external magnetic field to induce the magnetization switching, and the $-90°$ state and $90°$ state can be distinguished using different directions of the field.

We also studied the effect of magnetic anisotropy on switching. Magnetic anisotropy is one of the most important properties of metallic thin film magnets. The magnetization may display multi-step switching due to the different types of magnetic anisotropy.[19–21] For example, Yang *et al.*[22] reported multistep magnetic switching with single, double, and triple loops in single-crystal (001) Co_2MnGe Heusler alloy films resulted from a combined magnetic anisotropy consisting of cubic magnetocrystalline anisotropy and unaxial anisotropy. Based on the two possible I states, we obtained spin transfer multistep magnetization switching, which may be utilized in the design of multiple cell storage for high density STT-MRAM.

The magnetization dynamics is described using a generalized Landau-Lifshitz-Gilbert-Slonczewski (LLGS) equation[1,2]

$$\frac{d\mathbf{M}}{dt} = -\gamma'\mathbf{M}\times\mathbf{H}_{eff} - \frac{\alpha\gamma'}{M_s}\mathbf{M}\times(\mathbf{M}\times\mathbf{H}_{eff}) - \frac{2\mu_B J}{(1+\alpha^2)edM_s{}^3}g(\mathbf{M},\mathbf{P})\mathbf{M}\times(\mathbf{M}\times\mathbf{P}) + \frac{2\mu_B\alpha J}{(1+\alpha^2)edM_s{}^2}g(\mathbf{M},\mathbf{P})(\mathbf{M}\times\mathbf{P}), \quad (1)$$

where $\mathbf{M}$ is the magnetization of the free layer, $\mathbf{P}$ is the magnetization of the pinned layer, $\mathbf{H}_{\rm eff}$ is the effective field, $\gamma' = \gamma/(1+\alpha^2)$, γ is the electron gyromagnetic ratio, and α is the dimensionless damping parameter. The effective field includes the anisotropy field, the demagnetization field, the external field, and the exchange field, namely $\mathbf{H}_{\rm eff} = \mathbf{H}_{\rm k} + \mathbf{H}_{\rm d} + \mathbf{H}_{\rm ext} + \mathbf{H}_{\rm ex}$. In the STT term, $\mu_{\rm B}$, J, d, e, M_s, are the

a)Author to whom correspondence should be addressed. Electronic mail: xqma@sas.ustb.edu.cn. Tel.: +86-10-62334074. Fax: +86-10-62327283.

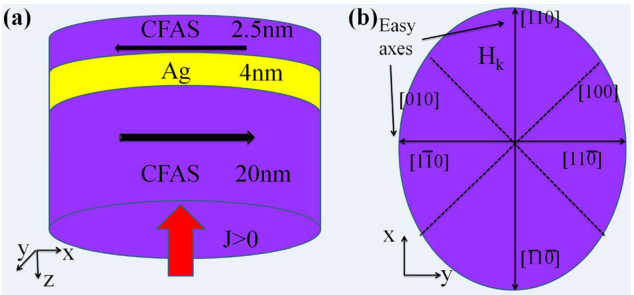

FIG. 1. (a) Model geometry definition of CFAS(2 nm)/Ag(4 nm)/CFAS(20 nm) nanopillar in Cartesian coordinates. (b) Cross section of the free layer for a coordinate transformation four-fold magnetocrystalline anisotropic field $\mathbf{H}_k$.

Bohr magneton, the current density, the thickness of the free layer, the electron charge, and the saturation magnetization, respectively. The scalar function[1] $g(\mathbf{M}, \mathbf{P})$ is given by $g(\mathbf{M}, \mathbf{P}) = [-4 + (1+\eta)^3(3 + \mathbf{M}\cdot\mathbf{P}/M_s^2)/4\eta^{3/2}]^{-1}$, where the angle between $\mathbf{M}$ and $\mathbf{P}$ is θ. $\mathbf{M}\cdot\mathbf{P}/M_s^2 = \cos\theta$.

We investigated a Heusler-based spin-valve nanopillar with the structure of CFAS (20 nm)/Ag (4 nm)/CFAS (2 nm) of elliptical cross section area (250×190 nm^2) as shown in Figure 1(a). We employed a Cartesian coordinate system where the current is along the z axis. We generally defined the positive current as electrons flowing from the free layer to the pinned layer. In this paper, the positive current will lead to the AP structure between the free layer and the pinned layer, while the negative current will lead to the P structure according to the STT theory. The initial pinned layer magnetization of 20 nm CFAS is along the +x axis, and the initial free layer magnetization of 2 nm CFAS is along +x or −x, depending on the current direction. The x-axis is the long axis of the ellipse along the CFAS [110] direction (easy axis) and the y-axis is along the short axis ([−110]) as shown in Figure 1(b). In this paper, the magnetic anisotropy energy $\mathbf{E}_k = K_1\alpha_1^2\alpha_2^2$, where K_1 is the cubic anisotropy constant, α_1 and α_2 are the direction cosines of θ for the in-plane four-fold magnetic anisotropy with respect to the in-plane cubic [100] and [010] axes at $\alpha_1 = \cos(\theta + 45°)$ and $\alpha_2 = \cos(\theta - 45°)$ for the four-fold magnetic anisotropy. We have two different kinds of magnetic anisotropy, a four-fold magnetic anisotropy similar to the experiment[14] and a 45° coordinate transformation four-fold magnetic anisotropy with different anisotropy constants.[19] From the experiment, the directions of [110] and [−110] are easy axes for the four-fold magnetic anisotropy. However, the directions of [100] and [010] should be easy axes for the coordinate transformation four-fold magnetic anisotropy.

The magnetic parameters employed in the simulations are[14,18] as follows: saturation magnetization $M_s = 9.0 \times 10^5$ A/m, exchange constant $A = 2.0 \times 10^{-11}$ J/m, Gilbert damping parameter $\alpha = 0.008$, spin polarization factor $\eta = 0.76$, magnetocrystalline anisotropy constant $K_1 = -1.0 \times 10^4$ J/m^3 for spin transfer two-step switching, and $K_1 = -3.0 \times 10^4$ J/m^3 for spin transfer multi-step switching. The anisotropy field should be sufficiently large that the anisotropy energy will overcome the demagnetization energy 4.0×10^3 J/m^3 to realize the specific three-step switching process.[14] The dynamics of magnetization was investigated by numerically solving the time-dependent LLGS equation using the Gauss-Seidel projection method[23–27] with a constant time step $\Delta t = 0.0238993$ ps. Simulations with a small time step produce essentially the same results. The samples were discretized in computational cells of $2 \times 2 \times 2$ nm^3.

Figures 2(a) and 2(b) show temporal evolutions of the average normalized magnetization components $\langle \mathbf{m_x} \rangle$, $\langle \mathbf{m_y} \rangle$ and $\langle \mathbf{m_z} \rangle$ ($\mathbf{m} = \mathbf{M}/M_s$) at the current densities of -4.0×10^6 A/cm^2 and -8.0×10^6 A/cm^2, respectively. The oscillations of $\langle m_x \rangle$ between two figures are switching from −1 to 0, and $\langle m_z \rangle$ is from 0 to 0. However, it is found that the magnetization component $\langle \mathbf{m_y} \rangle$ is −1.0 (−90° state) at -4.0×10^6 A/cm^2, while $\langle \mathbf{m_y} \rangle$ is 1.0 (90° state) at -8.0×10^6 A/cm^2. These two states

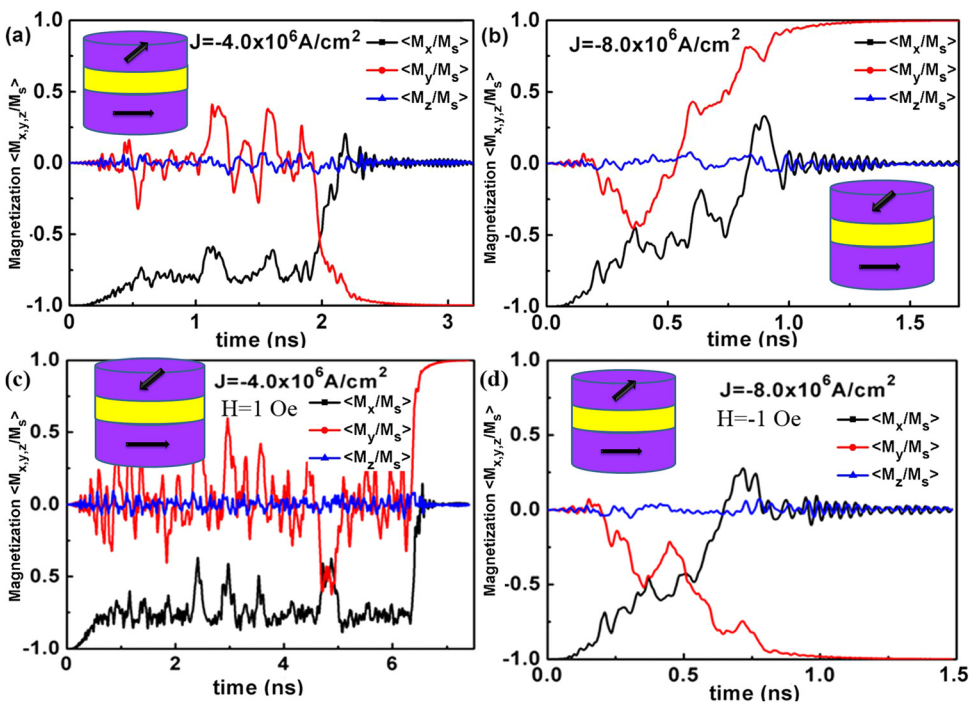

FIG. 2. Temporal evolutions of the average normalized magnetization components $\langle \mathbf{m_x} \rangle$, $\langle \mathbf{m_y} \rangle$, and $\langle \mathbf{m_z} \rangle$ for (a) −90° state at -4.0×10^6 A/cm^2, (b) 90° state at -8.0×10^6 A/cm^2, (c) 90° state at -4.0×10^6 A/cm^2 and 1 Oe, and (d) −90° state at -8.0×10^6 A/cm^2 and −1 Oe.

could not be observed and distinguished in the experiments because they have same resistance. If another magnetic layer is added in this spin-valve nanopillar, there will be resistance difference between −90° state and 90° state. As a matter of fact, we found the magnetization flips randomly to −90° state or 90° state with equal probability within the current range of $-4.0\times10^6\,A/cm^2 < J < -8.0\times10^6\,A/cm^2$ because switching to two states should overcome the same energy barrier of magnetic anisotropy. The degeneracy of the two states can be lifted by adding a small external magnetic field perturbation along +y or –y axis. As shown in Figures 2(c) and 2(d), it is found that the magnetization component $\langle \mathbf{m}_y \rangle$ is 1.0 (90° state) at $-4.0\times10^6\,A/cm^2$ and the magnetic field 1 Oe along the positive y axis while $\langle \mathbf{m}_y \rangle$ is −1.0 (−90° state) at $-8.0\times10^6\,A/cm^2$ and the magnetic field −1 Oe along the negative y axis. In addition, the thermal stability Δ_0, $\Delta_0 = K_1V/k_BT$, is about 86 at 300 K, where K_1, V, k_B, and T represent magnetic anisotropy constant, volume of the free layer, Boltzmann's constant, and temperature, respectively.[14]

Figure 3 shows snapshots of spin-transfer switching from AP to 90° state for a $250\times190\ nm^2$ ellipse under $-4.0\times10^6\,A/cm^2$ and 1 Oe. The colors represent different domain area, purple −x, blue +x, yellow −y, and green +y domains, respectively. Based on the domain structure evolution, we separate the magnetization switching process into two stages. In the first stage before 6.3 ns, it is multi-domains structure as shown in Figures 3(a)–3(c). This multi-domain evolution process could be explained by the large current input energy. The energy per unit time pumped into the nanopillar by the current is so large, that the formation of magnetic excitations with the wavelength much shorter than the element size becomes possible, leading to the formation of multi-domains. In the second stage, the free layer is switched to 90° state under the driving of current and the small external magnetic field. Furthermore, the value of STT at 90° state is not equal to zero since the magnetizations are along the y axis, and the angle between the free layer magnetization and the fixed layer magnetization is 90°. But this STT cannot overcome the fourfold in-plane magnetocrystalline anisotropy field and the external magnetic field.

We simulated the spin transfer multi-step switching in a full-Heusler CFAS alloy spin-valve nanopillar under a changed four-fold magnetic anisotropy which has 45° coordinate transformation. A combined magnetic anisotropy consisting of cubic magnetocrystalline anisotropy and unaxial anisotropy was fulfilled from the experiment of single-crystal (001) Co_2MnGe Heusler alloy films,[22] the easy axis having different degree coordinate transformation resulted single, double, and triple loops. We observed a multi-step hysteresis loop of resistance as a function of current density (Figure 4). We found 45° and 135° states due to the coordinate transformation four-fold magnetic anisotropy in addition to the AP and P states because the easy axis is along [100] and [010] directions. Three-step switching only exists in the current decrease process during which the magnetization switches from AP to P, while two-step switching appears in the current increase process where the magnetization switches from P to AP. For the three-step switching, the magnetization flips from AP to 135° state first at $1.0\times10^7\,A/cm^2$, 135° to 45° state at $-15.0\times10^7\,A/cm^2$, and 45° state to P state at $-30.0\times10^7\,A/cm^2$. In the two-step switching, the magnetization flips from P state to 45° state at $-10.0\times10^7\,A/cm^2$, then 45° state to AP state directly at $3.0\times10^7\,A/cm^2$. This unsymmetrical hysteresis loop is explained by the unsymmetrical curve of the effective field of the STT $\mathbf{H}_{stt} = 2\mu_B Jg(\mathbf{M},\mathbf{P})/(\gamma edM_s^3)$.[18,25] The switching current densities are of the order of 10^7–$10^8\,A/cm^2$ which are larger than the experimental result[14] and our previous simulation result[18] because of using the different magnetic anisotropy constant of Co_2MnGe.[22] The different magnetic anisotropy constants lead to different quantitative values of critical current; however, our simulation qualitatively captured the major features of multi-steps spin transfer switching.

Compared with previous multilevel bit spin transfer switching,[16,28] our results have several advantages. First, the smaller critical current density can be achieved in the Heusler-based alloy spin valve. Second, it may reduce the cost of magnetic device because only one soft layer is required during the design of multilevel bit spin transfer switching magnetic devices, while two soft layers (one is hard layer and the other is soft layer) are needed in the previous multilevel bit spin transfer switching device. Third, certain transitions are prohibited in the previous structures since the hard soft layer requires a

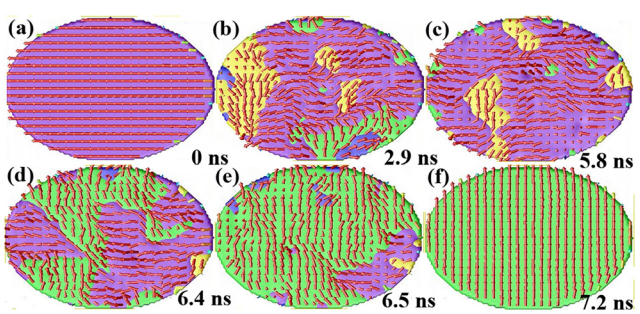

FIG. 3. Snapshots of magnetization distribution of the $250\times190\ nm^2$ ellipse. The colors represent the average magnetization component of $\langle \mathbf{m}_z \rangle$ (purple −x, blue +x, yellow −y, and green +y domains).

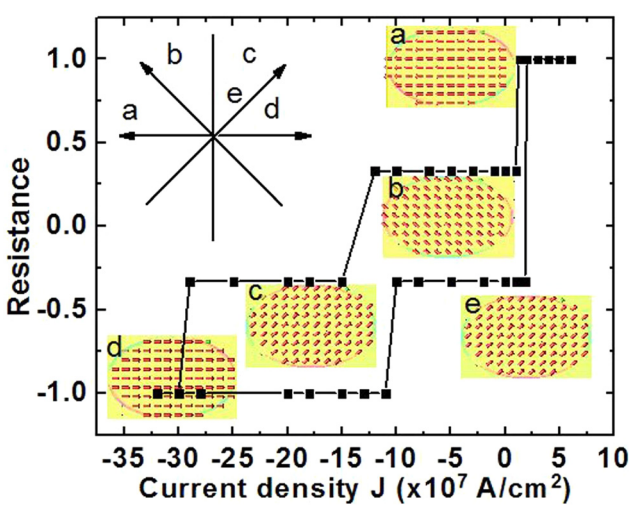

FIG. 4. The resistance as a function of current density (R-J) curves of CFAS/Ag/CFAS current perpendicular to the plane GMR nanopillar after the coordinate transformation of magnetic anisotropy. Insets also show the coordinate system and the domain structures (a–e). The colors of domains represent the average magnetization component of $\langle m_z \rangle$ (yellow equals to zero).

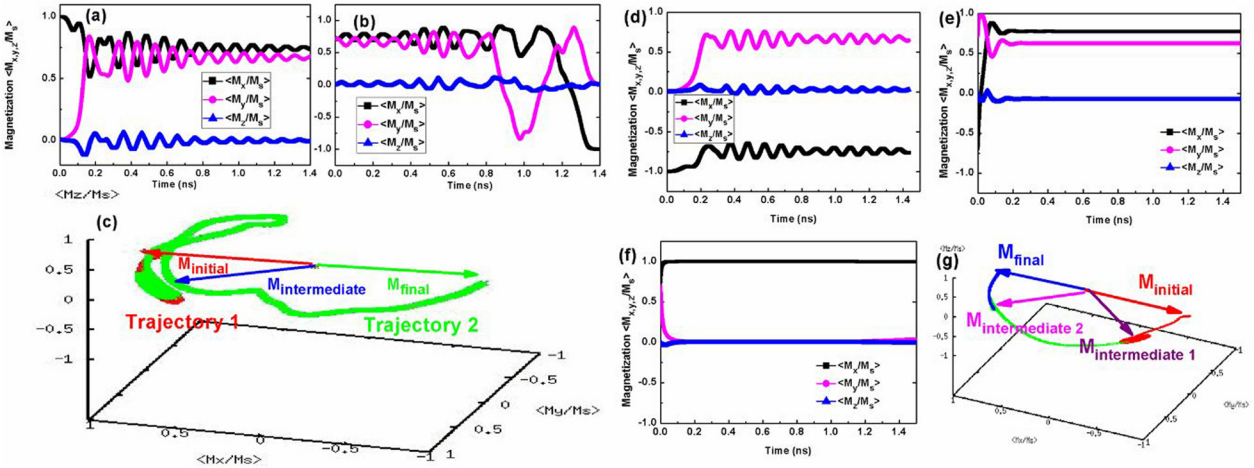

FIG. 5. Temporal evolutions of the average normalized magnetization components $\langle \mathbf{m_x} \rangle$, $\langle \mathbf{m_y} \rangle$, and $\langle \mathbf{m_z} \rangle$ (a) $0^\circ \rightarrow 45^\circ$ state at -1.0×10^7 A/cm^2, (b) $45^\circ \rightarrow 180^\circ$ state at 3.0×10^7 A/cm^2, (c) the trajectories from $0^\circ \rightarrow 45^\circ$ and $45^\circ \rightarrow 180^\circ$, (d) $180^\circ \rightarrow 135^\circ$ state at 7.0×10^6 A/cm^2, (e) $135^\circ \rightarrow 45^\circ$ state at -1.5×10^8 A/cm^2, (f) $45^\circ \rightarrow 0^\circ$ state at -3.0×10^8 A/cm^2, (g) the trajectories from $180^\circ \rightarrow 135^\circ$, $135^\circ \rightarrow 45^\circ$, and $45^\circ \rightarrow 0^\circ$.

large current to switch and the soft layer can be switched by a small current. For example, "11," "10," "01," and "00" are four resistance states, where the first digit refers to the hard soft layer. Level 00 cannot be switched into 10 state by using a single current. Only reversible transitions between 11 and 10, 01, and 00 can be achieved. However, all transitions among 0°, 45°, 135°, and 180° states can be obtained except the switching from $45^\circ \rightarrow 145^\circ$ at the increasing current.

Figures 5(a), 5(b) and 5(d), 5(e), 5(f) show the temporal evolutions of the average normalized magnetization components $\langle \mathbf{m_x} \rangle$, $\langle \mathbf{m_y} \rangle$, and $\langle \mathbf{m_z} \rangle$. All the transitions could complete in a nanosecond without the assistance of an external magnetic field, which would have a significant improvement for the application of fast data storage. Figures 5(c) and 5(g) show the continuous magnetization trajectories. The 0° state switched to the 45° state at a small current, then to the 180° state at a larger current. However, two intermediate states (45° and 135°states) which are related with the distinction of $+90^\circ$ and -90° states could be observed from $180^\circ \rightarrow 0^\circ$ switching. Furthermore, the intermediate states could be skipped if the input current is large enough to make the magnetization switching directly from $180^\circ \rightarrow 0^\circ$ or $0^\circ \rightarrow 180^\circ$. For example, the initial 180° state could switch to 135°, 45°, and 0° states at 7.0×10^6 A/cm^2, 2.0×10^8 A/cm^2, and 3.0×10^8 A/cm^2, respectively. Therefore, our simulation results are very helpful for designing four state magnetic memory devices with spin transfer multi-step switching. As shown in Figure 4, the magnetization will stay in 45° or 135° state at zero current, and we should use the large current input to keep the magnetization stay in 0° or 180° state. Although we did not use the magnetic field to assist the magnetic switching in our simulation, the magnetic field should be applied along the x axis to keep the magnetization stay in x axis in the future experiment since the x axis is not an easy axis. Based on the achievement of the coordinate transformation magnetic anisotropy in the experiment of Co_2MnGe Heusler alloy films,[22] we believe that it is not difficult to fulfill the four-step switching in the Heusler-based alloy CFAS spin valve in future experiment.

In summary, we investigated the spin transfer multi-step switching in a full-Heusler alloy CFAS spin-valve nanopillar using micromagnetic simulations. In spin transfer two-step switching, we found two possible directions, -90° state and 90° state, for the intermediate state, which could not be distinguished due to the same resistance in the experiment. We showed the magnetization flips to -90° state or 90° state with equal probability. We demonstrated that the degeneracy of the two intermediate states can be broken by an applied external magnetic field. We observed multi-domain structures due to the large current pumped into the nanopillar during the initial stage of switching. In addition, we demonstrated a spin-transfer multi-step magnetization switching through the coordinate transformation magnetic anisotropy and obtained the unsymmetrical hysteresis loops. All the transitions depending on the valve of current could be obtained among 0°, 45°, 135°, and 180° states except the switching from $45^\circ \rightarrow 145^\circ$ at the increasing current. The results may be utilized in designing four state magnetic memories driven by spin transfer torques.

This work was sponsored by the National Science Foundation of China (11174030), by the US National Science Foundation under the Grant No. DMR-1006541 (Chen) and in part by the China Scholarship Council. The computer simulations were carried out on the LION and Cyberstar clusters at the Pennsylvania State University.

[1]L. Berger, Phys. Rev. B **54**, 9353 (1996).
[2]J. C. Slonczewski, J. Magn. Magn. Mater. **159**, L1 (1996).
[3]S. I. Kiselev, J. C. Sankey, I. N. Krivorotov, N. C. Emley, R. J. Schoelkopf, R. A. Buhrman, and D. C. Ralph, Nature **425**, 380 (2003).
[4]T. Y. Chen, Y. Ji, C. L. Chien, and M. D. Stiles, Phys. Rev. Lett. **93**, 026601 (2004).
[5]W. H. Rippard, M. R. Pufall, S. Kaka, S. E. Russek, and T. J. Silva, Phys. Rev. Lett. **92**, 027201 (2004).
[6]S. Urazhdin, N. O. Birge, W. P. Pratt, and J. Bass, Phys. Rev. Lett. **91**, 146803 (2003).
[7]J. A. Katine, F. J. Albert, R. A. Buhrman, E. B. Myers, and D. C. Ralph, Phys. Rev. Lett. **84**, 3149 (2000).
[8]B. Özyilmaz, A. D. Kent, D. Monsma, J. Z. Sun, M. J. Rooks, and R. H. Koch, Phys. Rev. Lett. **91**, 067203 (2003).
[9]K. Aoshima, N. Funabashi, K. Machida, Y. Miyamoto, K. Kuga, and N. Kawamura, J. Magn. Magn. Mater. **310**, 2018 (2007).
[10]T. Furubayashi, K. Kodama, H. Sukegawa, Y. K. Takahashi, K. Inomata, and K. Hono, Appl. Phys. Lett. **93**, 122507 (2008).

[11]S. Trudel, O. Gaier, J. Hamrle, and B. Hillebrands, J. Phys. D: Appl. Phys. **43**, 193001 (2010).
[12]S. Mitani, J. Phys. D: Appl. Phys. **44**, 384003 (2011).
[13]T. Seki, S. Mitani, and K. Takanashi, Phys. Rev. B **77**, 214414 (2008).
[14]H. Sukegawa, S. Kasai, T. Furubayashi, S. Mitani, and K. Inomata, Appl. Phys. Lett. **96**, 042508 (2010).
[15]W. C. Jeong, B. I. Lee, and S. K. Joo, J. Appl. Phys. **85**, 4782 (1999).
[16]X. Lou, Z. Gao, D. V. Dimitrov, and M. X. Tang, Appl. Phys. Lett. **93**, 242502 (2008).
[17]T. Ishigaki, T. Kawahara, R. Takemura, K. Ona, K. Ito, H. Matsuoka, and H. Ohno, VLSI Tech. Dig. **2010**, 47.
[18]H. B. Huang, X. Q. Ma, Z. H. Liu, F. Y. Meng, Z. H. Xiao, P. P. Wu, S. Q. Shi, and L. Q. Chen, J. Appl. Phys. **110**, 033913 (2011).
[19]R. P. Cowburn, S. J. Gray, J. Ferre, J. A. C. Bland, and J. Miltat, J. Appl. Phys. **78**, 7210 (1995).
[20]K. He, D. J. Smith, and M. R. McCartney, Appl. Phys. Lett. **94**, 172503 (2009).
[21]Q. F. Zhan, S. Vandezande, K. Temst, and C. V. Haesendonck, Phys. Rev. B **80**, 094416 (2009).
[22]F. Y. Yang, C. H. Shang, C. L. Chien, T. Ambrose, J. J. Krebs, G. A. Prinz, V. I. Nikitenko, V. S. Gornakov, A. J. Shapiro, and R. D. Shull, Phys. Rev. B **65**, 174410 (2002).
[23]X. P. Wang, C. J. García-Cervera, and E. Weinan, J. Comput. Phys. **171**, 357 (2001).
[24]J. X. Zhang and L. Q. Chen, Acta Mater. **53**, 2845 (2005).
[25]Z. H. Xiao, X. Q. Ma, P. P. Wu, J. X. Zhang, L. Q. Chen, and S. Q. Shi, J. Appl. Phys. **102**, 093907 (2007).
[26]X. Q. Ma, Z. H. Xiao, P. P. Wu, J. X. Zhang, L. Q. Chen, and S. Q. Shi, J. Appl. Phys. **103**, 07B111 (2008).
[27]H. B. Huang, X. Q. Ma, T. Yue, Z. H. Xiao, S. Q. Shi, and L. Q. Chen, Sci. China, Ser. G **54**(7), 1227–1234 (2011).
[28]R. Sbiaa, R. Law, S. Y. H. Lua, E. L. Tan, T. Tahmasebi, C. C. Wang, and S. N. Piramanayagam, Appl. Phys. Lett. **99**, 092506 (2011).